µFLU14-142

RAREFIED GAS FLOW AND HEAT TRANSFER IN A MICROCAVITY HEATED BY A WALL HEAT FLUX

Giorgos Tatsios*[1], Dimitris Valougeorgis[1], Stefan K. Stefanov[2]
[1]Department of Mechanical Engineering, University of Thessaly, Volos, Greece
tatsios@mie.uth.gr, diva@mie.uth.gr
[2]Institute of Mechanics, Bulgarian Academy of Sciences, Sofia, Bulgaria
stefanov@imbm.bas.bg

KEY WORDS

Micro heat transfer, Shakhov model, DSMC, GASMEMS

ABSTRACT

The flow configuration in a 2D cavity where the three walls of the cavity are maintained at some constant temperature, while the fourth one is heated by a given heat flux distribution is considered. The problem is solved in a deterministic manner by the nonlinear Shakhov kinetic model and in a stochastic manner by the DSMC method in the whole range of the Knudsen number and for various heat fluxes resulting to small, moderate and large temperature differences between the cold and hot walls. Results include all macroscopic distributions of practical interest and very good agreement between kinetic modeling and DSMC results is obtained. Specific attention is given to the heat flux streamlines and contours and to further analyze the flow and thermal configuration in the cavity a recently introduced decomposition of the solution into ballistic and collision parts is applied. It is found that the heat flux provided in one wall is not a monotonic function of the ratio of the temperature of the three cold walls and the resulting temperature of the hot wall.

1. INTRODUCTION

Thermally induced rarefied gas flows in cavities have lately received considerable attention, due to their implementation in several technological fields including cooling processes of vacuum packed MEMS [1], micropumps/microactuators [2,3] and vacuum sensors [4]. They also serve as prototype flow/thermal configurations to study novel non-equilibrium phenomena. Recently, in addition to the typical cold-to-hot thermal creep type flow, an unexpected hot-to-cold flow along the walls has been observed [5,6]. This latter type of flow has been thoroughly investigated and theoretically explained in [7] by decomposing the distribution function and the deduced macroscopic quantities into ballistic and collision segments. In all works presented so far the temperature of the cold and hot cavity walls are given to form the proper set of boundary conditions to close the problem.

Within this framework, here, the thermally induced flow in a square cavity, where the three walls are maintained at some constant temperature, while the fourth one is heated (or cooled) by a given heat flux distribution is considered. The temperature of the heated wall is part of the solution. Thus, this work with the modified boundary condition may be considered as a continuation of the previous works [6,7] and it may be useful in occasions where instead of the wall temperature is easier for practical purposes to measure the heat flux heating or cooling the wall. Modelling is based on the non-linear Shakhov model [8], while the DSMC approach [9] is used to benchmark the solution as well as to apply the distribution function decomposition methodology and to split the heat flux into ballistic and collision parts in an effort to have a more thorough view of the heat flow field.

* Corresponding author

2. FLOW CONFIGURATION

A rarefied monatomic gas is contained in a 2D square enclosure of side length W. The space variables are denoted by (x', y') with $-W/2 \le x' \le W/2$ and $0 \le y' \le W$. The three walls of the cavity are kept at a constant temperature T_C, while the fourth wall is heated by a constant heat flux of given magnitude Q_H. The temperature distribution along the heated wall is denoted by T_H and is part of the solution. Thus, there is a steady-state heat flow through the enclosed gas defined by the heat flux vector $\boldsymbol{Q} = \left[Q_x(x', y'), Q_y(x', y')\right]$. Also, due to non-equilibrium phenomena, a flow field, defined by the two component velocity vector $\boldsymbol{U} = \left[U_x(x', y'), U_y(x', y')\right]$, is deduced, as well. It is noted that gravitational forces are not considered. The gas temperature and density distributions are denoted by $T(x', y')$ and $N(x', y')$ respectively, while the pressure is given by the equation of state $P = Nk_B T$, where k_B is the Boltzmann constant.

It is convenient to solve the problem in terms of the following dimensionless quantities:

$$x = \frac{x'}{W},\quad y = \frac{y'}{W},\quad n = \frac{N'}{N_0},\quad \tau = \frac{T'}{T_0},\quad p = \frac{P}{P_0},\quad u_x = \frac{U_x}{\upsilon_0},\quad u_y = \frac{U_y}{\upsilon_0},\quad q_x = \frac{Q_x}{P_0\upsilon_0},\quad q_y = \frac{Q_y}{P_0\upsilon_0}. \tag{1}$$

The quantities n, τ, p, (u_x, u_y) and (q_x, q_y) are the two dimensional distributions of number density, temperature, pressure and the two components of the velocity and heat flux vectors respectively, while the space variables are $x \in [-1/2, 1/2]$ and $y \in [0,1]$. The quantities with zero subscript are the corresponding reference quantities with $P_0 = N_0 k_B T_0$ and $\upsilon_0 = \sqrt{2k_B T_0 / m}$, with m denoting the molecular mass, denoting the most probable molecular velocity. The hard sphere model is used to simulate intermolecular collisions. The problem is characterized by two parameters, namely the reference Knudsen number, defined as

$$Kn_0 = \frac{\sqrt{\pi}}{2}\frac{\mu_0 u_0}{P_0 W}. \tag{2}$$

where μ_0 is the viscosity at reference temperature T_0 and the dimensionless magnitude of the heat flux departing from the heated denoted by $q_H = Q_H / (P_0\upsilon_0)$. In the results section the effect of these parameters on the flow is investigated. As noted before the problem is modeled by the nonlinear Shakhov kinetic equation and the DSMC method both described in the next section.

3. DETERMINISTIC AND STOCHASTIC MODELING

3.1 Deterministic modeling based on the Shakhov kinetic model

The dimensionless steady-state 2D Shakhov kinetic model equation, following the well-known projection procedure is written as [7]

$$\zeta_x \frac{\partial \varphi}{\partial x} + \zeta_y \frac{\partial \varphi}{\partial y} = \frac{\sqrt{\pi}}{2}\frac{1}{Kn_0} n\sqrt{\tau}\left(\varphi^S - \varphi\right), \quad \zeta_x \frac{\partial \psi}{\partial x} + \zeta_y \frac{\partial \psi}{\partial y} = \frac{\sqrt{\pi}}{2}\frac{1}{Kn_0} n\sqrt{\tau}\left(\psi^S - \psi\right). \tag{3}$$

with (ζ_x, ζ_y) denoting the two components of the molecular velocity vector and

$$\varphi^S = \varphi^M\left[1 + \frac{4}{15}\frac{1}{n\tau^2}\left[q_x(\zeta_x - u_x) + q_y(\zeta_y - u_y)\right]\left(\left[(\zeta_x - u_x)^2 + (\zeta_y - u_y)^2\right]/\tau - 2\right)\right]. \tag{4}$$

$$\psi^S = \psi^M\left[1 + \frac{4}{15}\frac{1}{n\tau^2}\left[q_x(\zeta_x - u_x) + q_y(\zeta_y - u_y)\right]\left(\left[(\zeta_x - u_x)^2 + (\zeta_y - u_y)^2\right]/\tau - 1\right)\right]. \tag{5}$$

while the reduced local Maxwellians are

$$\varphi^M = \frac{n}{\pi\tau}\exp\left[-\left[(\zeta_x - u_x)^2 + (\zeta_y - u_y)^2\right]/\tau\right], \quad \psi^M = \frac{n}{2\pi}\exp\left[-\left[(\zeta_x - u_x)^2 + (\zeta_y - u_y)^2\right]/\tau\right]. \tag{6}$$

The macroscopic quantities are given as moments of the reduced distribution functions φ and ψ:

$$n(x,y)=\int_{-\infty}^{\infty}\int_{-\infty}^{\infty}\varphi d\zeta_x d\zeta_y\,,\quad u_x(x,y)=\frac{1}{n}\int_{-\infty}^{\infty}\int_{-\infty}^{\infty}\zeta_x\varphi d\zeta_x d\zeta_y\,,\quad u_y(x,y)=\frac{1}{n}\int_{-\infty}^{\infty}\int_{-\infty}^{\infty}\zeta_y\varphi d\zeta_x d\zeta_y\,. \tag{7}$$

$$\tau(x,y)=\frac{2}{3n}\int_{-\infty}^{\infty}\int_{-\infty}^{\infty}\left[\left(\zeta_x^2+\zeta_y^2\right)\varphi+\psi\right]d\zeta_x d\zeta_y-\frac{2}{3}\left(u_x^2+u_y^2\right). \tag{8}$$

$$\boldsymbol{q}(x,y)=\left(q_x,q_y\right)=\int_{-\infty}^{\infty}\int_{-\infty}^{\infty}\left[\left[\left(\zeta_x-u_x\right)^2+\left(\zeta_y-u_y\right)^2\right]\varphi+\psi\right]\left(\boldsymbol{\zeta}-\boldsymbol{u}\right)d\zeta_x d\zeta_y\,. \tag{9}$$

The purely diffuse Maxwell boundary conditions have been implemented. The outgoing distribution at the boundaries denoted by φ^+ and ψ^+, are expressed as [7]

$$\varphi^+=\frac{n_w}{\pi\tau_w}\exp\left[-\left(\zeta_x^2+\zeta_y^2\right)/\tau_w\right]\,,\quad \psi^+=\frac{n_w}{2\pi}\exp\left[-\left(\zeta_x^2+\zeta_y^2\right)/\tau_w\right]. \tag{10}$$

where n_w is a parameter calculated in terms of the ingoing distributions, satisfying the impermeability wall conditions and τ_w is the dimensionless wall temperature. This latter parameter is known for the three walls kept at temperature T_C and unknown at the wall which is heated by the heat flux q_H. To close the problem an additional expression is obtained for τ_w at the heated wall by satisfying the relation that the normal heat flux at the heated wall must be equal to q_H. In the present work, without loss of generality, the heated wall is at $y=0$ and therefore

$$q_y(x,0)=q_H\,. \tag{11}$$

Equation (11) along with the no penetration condition yields

$$\tau_w=\frac{1}{2}\left(\frac{B-q_H}{A}\right)\,,\quad n_w=-2A\left(\frac{\pi}{\tau_w}\right)^{1/2}. \tag{12}$$

where

$$A=\int_{-\infty}^{0}\int_{-\infty}^{\infty}\zeta_y\varphi^- d\zeta_x d\zeta_y\,,\quad B=\int_{-\infty}^{0}\int_{-\infty}^{\infty}\left[\left[\left(\zeta_x-u_x\right)^2+\left(\zeta_y-u_y\right)^2\right]\varphi^-+\psi^-\right]\left(\zeta_y-u_y\right)d\zeta_x d\zeta_y\,. \tag{13}$$

with φ^- and ψ^- denoting the ingoing distributions.

The above set of integro-differential equations (3) coupled with the expressions (4-9) subject to boundary conditions (10) are solved numerically discretizing by the control volume approach in the physical space and the discrete velocity method in the molecular velocity space. The implemented algorithm has been utilized the solve nonlinear flows and heat transfer problems with considerable success [7,10,11]. In the present work the iterative process of the algorithm is terminated when the imposed termination criteria

$$\varepsilon^{(k)}=\max_{i,j}\left\{\left|n_{i,j}^{(k)}-n_{i,j}^{(k-1)}\right|+\left|u_{xi,j}^{(k)}-u_{xi,j}^{(k-1)}\right|+\left|u_{yi,j}^{(k)}-u_{yi,j}^{(k-1)}\right|+\left|\tau_{i,j}^{(k)}-\tau_{i,j}^{(k-1)}\right|\right\}\le 10^{-10}\,. \tag{14}$$

where k denotes the iteration index and $\varepsilon^{(k)}$ the error after k iterations, is fulfilled. It is noted that upon convergence all conservation principles are accordingly preserved.

3.2 Stochastic modeling based on the DSMC method

The DSMC method is based on splitting the real process of particle motion in two consecutive steps: a) the collision between the particles which is modeled in a stochastic manner within the particles at a given cell, and b) the ballistic motion of the particles over a distance proportional to their velocities, which is purely deterministic. The traditional No Time Counter (NTC) scheme [9] together with the HS molecular interaction model, are used for computing the collision between two particles. The implementation of the given heat flux boundary condition is according to the methodology described in [12]. The interaction of the gas molecules with the solid walls is assumed to be purely diffuse. Here, the space domain is discretized into 100x100 squared cells with size smaller than the mean free path, while the gas is represented by a discrete number of 10^5 - 10^6 model particles, depending upon the parameters and the time step is chosen to be about 1/3 of the cell traversal time. The sampling of the macroscopic quantities starts once the steady state flow has been achieved and is carried out by volume based time averaging of the corresponding microscopic values of the particles in larger sampling cells that represent groups of 4 x 4 neighboring collision cells. These moments are accumulated over (5-15).10^5 time steps. This gives a sample size of approximately 10^9 -10^{10}

samples per sampling cell which is sufficiently large to reduce the statistical scatter of the macroscopic results.

In general, a kinetic solution at some point in a flow domain consists of two parts, namely the ballistic and the collision parts. The former one is due to particles arriving at this point from the boundaries of the flow domain with no collisions, while the latter one is due to particles arriving at this point after an arbitrary number of collisions (at least one). The decomposition of the particle distribution in a given cell of the computational grid can be implemented in the basic DSMC algorithm by making some additions in the indexing stage. More specifically, all model particles $j = 1,\ldots,N_T$ taking place in the simulation are tagged by introducing the indicator I_j, which has the value of 0 or 1 indicating if a particle contributes to the ballistic or the collision part of the distribution respectively. A particle passes into the ballistic part when it is reflected from a wall and goes into the collision part when it interacts with another particle. The indicator is set to 0 each time that a particle is reflected from the bounding walls of the enclosure, while in the stage of particle free motion the indicators are not changed. In the stage of binary collisions the indicators $\left(I_j, I_k\right)$ of any pair of particles $\left(j,k\right)$ involved in a collision are set to 1. During the simulation process the particle indicators may change their values all the time. In the sampling stage of the macroscopic properties at given time t_k all particles with indicators $I_j = 0$, are considered belonging to the ballistic part of the particle distribution and all particles with indicators $I_j = 1$ to the collision part. As a result, the total number of all particles accumulated in a cell is divided into two groups $N_T = N^{(b)} + N^{(c)}$ and the macroscopic quantities are sampled into the two corresponding parts. Here, we are interested mainly in the bulk velocity and heat flux components. For brevity, we illustrate the sampling by giving the ballistic and collision parts of x-components of velocity and heat flux:

$$u_x^{(b)} = \frac{1}{N_T}\sum_{k=1}^{S}\sum_{i=1}^{N(t_k)}\left[1 - I_i\left(t_k\right)\right]\zeta_{x,i}\left(t_k\right)\ ,\ u_x^{(c)} = \frac{1}{N_T}\sum_{k=1}^{S}\sum_{i=1}^{N(t_k)} I_i\left(t_k\right)\zeta_{x,i}\left(t_k\right). \tag{15}$$

$$\begin{aligned}\frac{q_x^{(b)}}{2} = {} & \frac{1}{N_T}\sum_{k=1}^{S}\sum_{i=1}^{N(t_k)}\left[1 - I_i\left(t_k\right)\right]\zeta_{x,i}\left(\zeta_{x,i}^2 + \zeta_{y,i}^2 + \zeta_{z,i}^2\right) - u_x\left\{\frac{1}{N_T}\sum_{k=1}^{S}\sum_{i=1}^{N(t_k)}\left[1 - I_i\left(t_k\right)\right]\left(\zeta_{x,i}^2 + \zeta_{y,i}^2 + \zeta_{z,i}^2\right)\right\} \\ & - 2u_x\left\{\frac{1}{N_T}\sum_{k=1}^{S}\sum_{i=1}^{N(t_k)}\left[1 - I_i\left(t_k\right)\right]\zeta_{x,i}^2\right\} - 2u_y\left\{\frac{1}{N_T}\sum_{k=1}^{S}\sum_{i=1}^{N(t_k)}\left[1 - I_i\left(t_k\right)\right]\zeta_{x,i}\zeta_{y,i}\right\} \\ & + \left(u_x^2 + u_y^2 + u_z^2\right)\left(u_x^{(b)} - n^{(b)}u_x\right) + 2u_x\left(u_x u_x^{(b)} + u_y u_y^{(b)}\right).\end{aligned} \tag{16}$$

$$\begin{aligned}\frac{q_x^{(c)}}{2} = {} & \frac{1}{N_T}\sum_{k=1}^{S}\sum_{i=1}^{N(t_k)}\zeta_{x,i}\left(\zeta_{x,i}^2 + \zeta_{y,i}^2 + \zeta_{z,i}^2\right) - u_x\left\{\frac{1}{N_T}\sum_{k=1}^{S}\sum_{i=1}^{N(t_k)} I_i\left(t_k\right)\left(\zeta_{x,i}^2 + \zeta_{y,i}^2 + \zeta_{z,i}^2\right)\right\} \\ & - 2u_x\left\{\frac{1}{N_T}\sum_{k=1}^{S}\sum_{i=1}^{N(t_k)} I_i\left(t_k\right)\zeta_{x,i}^2\right\} - 2u_y\left\{\frac{1}{N_T}\sum_{k=1}^{S}\sum_{i=1}^{N(t_k)} I_i\left(t_k\right)\zeta_{x,i}\zeta_{y,i}\right\} \\ & + \left(u_x^2 + u_y^2 + u_z^2\right)\left(u_x^{(c)} - n^{(c)}u_x\right) + 2u_x\left(u_x u_x^{(c)} + u_y u_y^{(c)}\right).\end{aligned} \tag{17}$$

Here, S denoted the number of samples, t_k indicates the different times over which the sampling is performed and $N\left(t_k\right)$ is the number of particles in the cell at time t_k. It is noted that the macroscopic properties are obtained by time averaging over $S = 5\times10^5$ time steps after the steady-state regime has been recovered. The y- components of velocity and heat flux are computed in the same way, by using the corresponding projections. Note that number density, bulk velocity and heat flux are equal to $n = n^{(b)} + n^{(c)}$, $\boldsymbol{u} = \boldsymbol{u}^{(b)} + \boldsymbol{u}^{(c)}$ and $\boldsymbol{q} = \boldsymbol{q}^{(b)} + \boldsymbol{q}^{(c)}$, respectively. For more details on the decomposition of the solution into ballistic and collision parts, see Ref. [7].

4. RESULTS AND DISCUSSION

Results are provided in a wide range of the reference Knudsen number Kn_0 and for various heat fluxes q_H, resulting to small, moderate and large temperature differences between the constant temperature T_C of the three walls and the deduced average temperature of the wall where the heat flux is defined as

$\bar{T}_H = \int_{-W/2}^{W/2} T_H(x')dx'$ once the unknown wall temperature $T_H(x')$ is computed. A comparison between kinetic results obtained by the Shakhov model and corresponding DSMC results is also performed, while the latter method is used to compute the ballistic and collision segments of the heat flow field.

A view of the flow configuration may be observed in Fig.1, where the streamlines and the temperature contours are provided for $Kn_0 = [0.1,1,10]$ and various q_H. It is noted that the given heat fluxes result to temperature ratios $T_C / \bar{T}_H = 0.1$ in Figs.1a-1c and 0.9 Figs.1d-1f respectively. As expected the flow is symmetric about $x' = 0$. It is seen that in all cases, along the walls, in addition to the two thermal creep type vortices, characterized by cold-to-hot flow, there are two additional counter rotating vortices with the gas flowing from hot-to-cold regions. These latter vortices as the reference Knudsen number is increased occupy larger areas of the cavity flow domain. The temperature variation along the bottom (heated) plate may be also seen. In most cases, particularly for $Kn_0 = [1,10]$, the temperature remains almost constant along the wall with some variations at the two edges of the wall. The gas velocity along the lateral wall, maintained at T_C, is shown in Fig.2. In most cases the distributions are positive indicating a flow motion from the hot to the cold region along the walls as it is also seen in Fig.1. Only very close to the two bottom edges there is motion in the opposite direction.

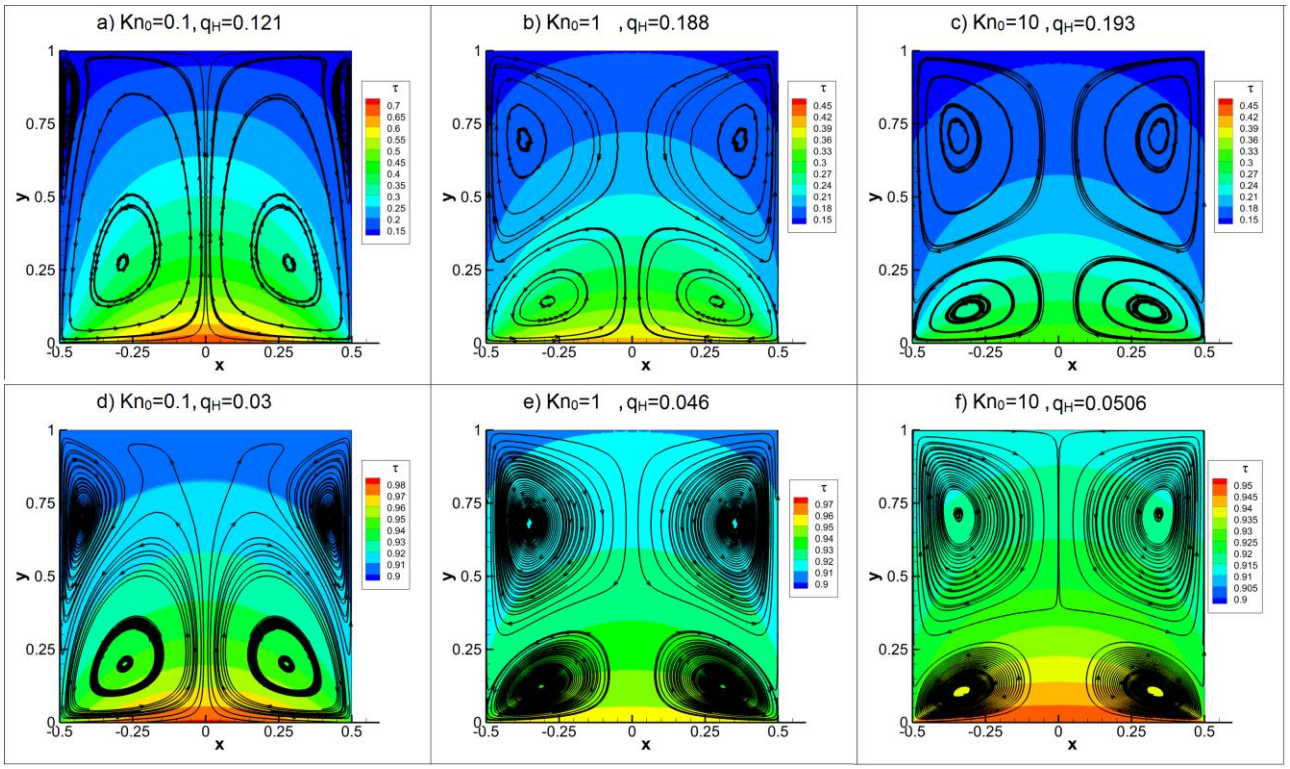

Figure 1: Streamlines and temperature contours for various values of the reference Knudsen number Kn_0 and heat fluxes q_H. The deduced ratios $T_C / \bar{T}_H$ are 0.1 (up) and 0.9 (down).

In Fig.3 the computed $T_C / \bar{T}_H$ are shown in terms of q_H for various Kn_0 from the slip through the transition down to the free molecular regimes. It is interesting to note that for a given q_H two different values of $T_C / \bar{T}_H$ may be obtained. This is in agreement with previous results reported in [6]. More specifically, initially as $T_C / \bar{T}_H$ is increased, q_H is also increased reaching its maximum value at some temperature ratio, which is around $T_C / \bar{T}_H = 0.3$ and then as $T_C / \bar{T}_H$ is further increased, q_H is decreased. This nonmonotonic behavior of q_H in terms of $T_C / \bar{T}_H$ occurs for all Knudsen numbers studied and it is more evident as Kn_0 is increased.

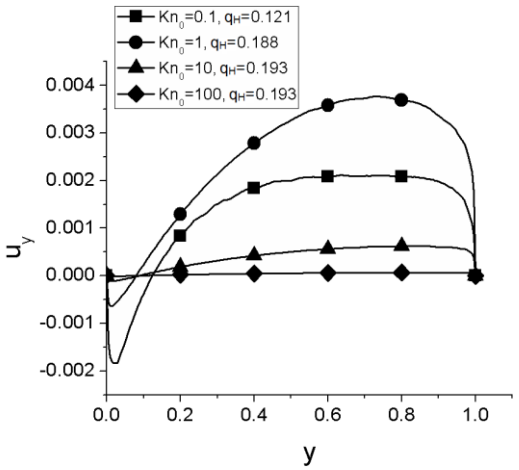

Figure 2: The vertical component of the macroscopic velocity along the lateral walls for various heat fluxes q_H and various reference Knudsen numbers Kn_0.

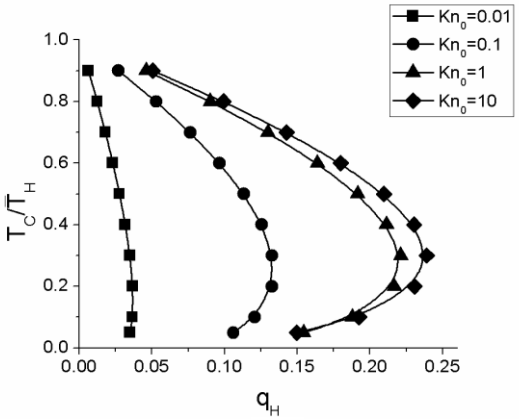

Figure 3: Temperature ratio $T_C / \bar{T}_H$ in terms of the dimensionless heat flux q_H for various reference Knudsen numbers Kn_0.

All above results have been obtained based on the direct solution of the Shakhov kinetic model. A detailed comparison with corresponding DSMC results presented in Tab.1 has been performed. As it is seen there is very good agreement between the two approaches.

Table 1: Comparison between kinetic and DSMC results in terms of q_H for various Kn_0 and $T_C / \bar{T}_H$

Kn_0	$T_C / \bar{T}_H$									
	0.05		0.1		0.3		0.5		0.9	
	Kinetic	DSMC	Kinetic	DSMC	Kinetic	DSMC	Kinetic	DSMC	Kinetic	DSMC
0.1	0.109	0.109	0.121	0.120	0.133	0.132	0.113	0.113	0.0270	0.0274
1	0.154	0.154	0.188	0.188	0.221	0.221	0.192	0.191	0.0459	0.0459
10	0.150	0.150	0.193	0.193	0.239	0.239	0.210	0.210	0.0506	0.0504

Furthermore, the DSMC method is used, to compute, as described in Section 3.2, the ballistic and collision segments of the heat flow field. In Fig.4 the heat flux lines of the ballistic and collision parts as well as of the overall solution obtained by adding the two parts are plotted for $Kn_0 = 1$ and for several $T_C / \bar{T}_H = [0.05, 0.1, 0.3, 0.5, 0.9]$. The corresponding contours of the vertical heat flux component q_y are also plotted. It is clearly seen that as $T_C / \bar{T}_H$ is increased, i.e., as the temperature difference between the hot and cold walls is decreased, the curvature and concentration of the ballistic and collision heat flux lines are becoming similar. This is evident for $T_C / \bar{T}_H = 0.5$ and 0.9. Of course their direction is opposite, i.e., the ballistic heat flux lines are starting from the walls and moving towards a focal point, while the collision heat flux lines are starting from a focal point and are moving towards the walls following however similar paths. Also, as $T_C / \bar{T}_H$ is increased the focal regions (points) of the ballistic and collision heat flux lines are moving from top and bottom respectively to the center of the cavity. In the limiting case of $T_C / \bar{T}_H = 1$ the focal points are at the cavity center and the two fields counter balanced each other deducing an overall solution (as it should) equal to zero. This symmetry is gradually lost as the temperature ratio is decreased. Thus, for $T_C / \bar{T}_H = 0.05$ and 0.1 both ballistic and collision parts have almost everywhere, except a small area of the collision part at the bottom, $q_y > 0$, while for $T_C / \bar{T}_H > 0.1$, q_y may be positive or negative.

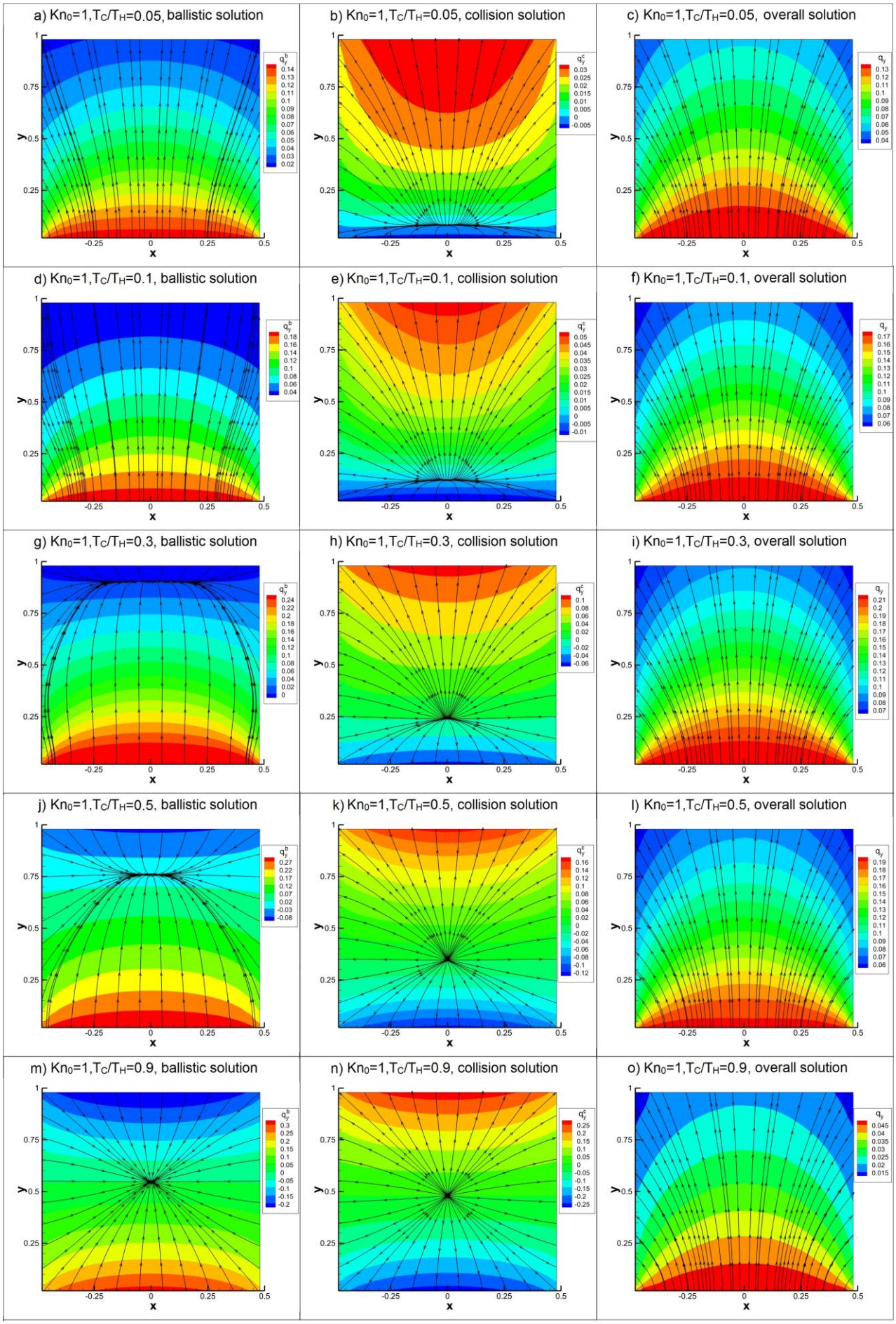

Figure 4: Heat flux lines and vertical component of the heat flux contours of the ballistic (left), collision (middle) parts as well as of the overall solution (right) for $Kn_0 = 1$ and various temperature ratios.

It is noted that although $T_C / \bar{T}_H$ has a significant effect on the two parts of the solution, it has a relatively small effect in the overall solution, where as it is seen in Fig.4, there is a strong qualitative resemblance between the overall heat flux lines for all temperature ratios. In all cases the heat flux lines are departing from the bottom heated plate and they are directed mainly towards the upper plate, while some of the them are reaching the side walls.

In Fig.5, the heat flux lines and the q_y contours are shown for $Kn_0 = 0.1$ and $T_C / \bar{T}_H = 0.5$. By comparing these results with the corresponding ones in Fig.4 it is seen that the effect of the gas rarefaction is important altering the structure of the ballistic and collision heat flux streamlines.

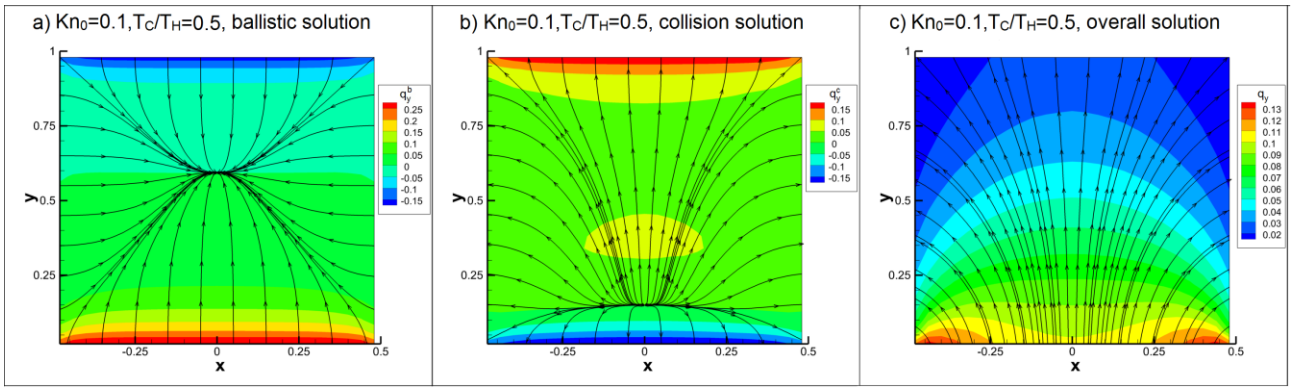

Figure 5: Heat flux lines and vertical component of the heat flux contours of the ballistic (left), collision (middle) parts as well as of the overall solution (right) for $Kn_0 = 0.1$ and $T_C / T_H = 0.5$.

The rarefied gas flow and thermal configuration in a square cavity with the three walls maintained at some constant temperature and the fourth wall heated by a known heat flux has been solved via kinetic modeling in a wide range of the Knudsen number. It is believed that the present research work has both scientific interest and technological impact and it may support the design and optimization of MEMS devices operating far from local equilibrium.

ACKNOWLEDGEMENTS

This project has received funding from the European Union's Horizon 2020 research and innovation programme under grant agreement number 633053. The views and opinions expressed herein do not necessarily reflect those of the European Commission.

REFERENCES AND CITATIONS

[1] Liu, H., Wang, M., Wang, J., Zhang, X. (2007). Monte Carlo simulations of gas flow and heat transfer in vacuum packed MEMS devices. *Applied Thermal Engineering*, **27**, 323-329.

[2] Alexeenko, A., Gimelshein, S., Muntz, E., Ketsdever A. (2006). Kinetic modeling of temperature driven flows in short microchannels. *International Journal of Thermal Sciences*, **45**, 1045-1051.

[3] Ketsdever, A., Gimelshein, N., Gimelshein, S., Selden, N. (2012). Radiometric phenomena: From the 19th to the 21st century. *Vacuum*, **86**, 1644-1662.

[4] Vargas, M., Wüest, M., Stefanov, S. (2012). Monte Carlo analysis of thermal transpiration effects in capacitance diaphragm gauges with helicoidal baffle system. *Journal of Physics:* Conference **362**, 012013.

[5] Rana, A., Torrilhon, M., Struchtrup, H. (2012). Heat transfer in micro devices packaged in partial vacuum. *Journal of Physics:* Conference Series, **362**, 012034.

[6] Tatsios, G., Vargas, M., Valougeorgis, D., Stefanov, S., Non-equilibrium gas flow and heat transfer in a bottom heated square microcavity, 4th Micro and Nano Flows Conference (MNF2014), London, UK, Sept. 7-10 (2014).

[7] Vargas, M., Tatsios, G., Valougeorgis, D., Stefanov, S. (2014). Rarefied gas flow in a rectangular enclosure induced by non-isothermal walls. *Physics of Fluids*, **26**, 057101.

[8] Shakhov, E. M. (1968). Generalization of the Krook kinetic relaxation equation. *Fluid Dynamics*, **3 (5)**, 142-145.

[9] Bird, G. A. (1994). *Molecular Gas Dynamics and the Direct Simulation of Gas Flows.* Oxford: Clarendon Press.

[10] Pantazis, S., Valougeorgis, D. (2010). Nonlinear heat transfer through rarefied gases between coaxial cylindrical surfaces at different temperatures. *European Journal of Mechanics B/Fluids*, **29**, 494-509.

[11] Pantazis, S., Naris, S., Tantos, C., Valougeorgis, D., Andre, J., Millet, F., Perin, J. P. (2013). Nonlinear vacuum gas flow through a short tube due to pressure and temperature gradients. *Fusion Engineering and Design*, **88**, 2384-2387.

[12] Akhlaghi, H., Roohi, E., Stefanov, S. (2012). A new iterative wall heat flux specifying technique in DSMC for heating/cooling simulations of MEMS/NEMS. *International Journal of Thermal Sciences*, **59**, 111-125.